Preprint typeset in JHEP style - HYPER VERSION

MCnet/08/05
LU-TP 08-14

Elastic and quasi-elastic pp and $\gamma^\star p$ scattering in the Dipole Model*

arXiv:0807.0325v1 [hep-ph] 2 Jul 2008

Christoffer Flensburg[†], **Gösta Gustafson**[†§] **and Leif Lönnblad**[†]

[†] *Dept. of Theoretical Physics, Sölvegatan 14A, S-223 62 Lund, Sweden*
[§] *II. Institut für Theoretische Physik, Universität Hamburg, Luruper Chaussee 149, 22761 Hamburg, Germany*
E-mail: christoffer.flensburg@thep.lu.se, gosta.gustafson@thep.lu.se *and* leif.lonnblad@thep.lu.se

Abstract: We have in earlier papers presented an extension of Mueller's dipole cascade model, which includes sub-leading effects from energy conservation and running coupling as well as colour suppressed saturation effects from pomeron loops via a "dipole swing". The model was applied to describe the total and diffractive cross sections in pp and $\gamma^* p$ collisions, and also the elastic cross section in pp scattering.
In this paper we extend the model to describe the corresponding quasi-elastic cross sections in $\gamma^* p$, namely the exclusive production of vector mesons and deeply virtual compton scattering. Also for these reactions we find a good agrement with measured cross sections. In addition we obtain a reasonable description of the t-dependence of the elastic pp and quasi-elastic $\gamma^\star p$ cross sections.

Keywords: Small-x physics, Saturation, Diffraction, Dipole Model, DIS.

*Work supported in part by the Marie Curie RTN "MCnet" (contract number MRTN-CT-2006-035606), by the Swedish Foundation for International Cooperation and Higher Education – STINT (contract number 2006/080) and by the Deutsche Forschungsgemeinschaft.

Contents

1. Introduction

We have in a series of papers [1–3] presented an extention of Mueller's dipole cascade model [4–6] implemented in a Monte Carlo program, which includes sub-leading effects from energy conservation and running coupling, as well as colour suppressed effects from pomeron loops via a *dipole swing* mechanism. It also includes a consistent treatment of non-perturbative confinement effects, which suppress dipoles with large transverse extension.

The advantage of a cascade model formulated in transverse coordinate space is the possibility to include effects of multiple collisions and saturation in a straight forward way. While analytic results have mainly been presented for the asymptotic behavior of total and diffractive cross sections, Monte Carlo simulations facilitate studies of non-leading effects and more quantitative results. A simulation of Mueller's initial model was presented by Salam in ref. [7]. Although giving finite results for the total cross section, this leading log evolution suffers from divergences for small dipoles, which caused numerical problems with very large gluon multiplicities and prevented simulations at higher energies. One important result from this analysis was the very large fluctuations in the evolution [8]. As the ratio between the elastic and the total cross sections is determined by the fluctuations in the scattering process, this implies that less fluctuations is needed in the impact parameter dependence, to reproduce the experimental data. As a result we found in ref. [3] that including the fluctuations in the evolution implies that the impact parameter profile is not as "black and white" as in analyses where only fluctuations in the impact parameter are taken into account.

In the model described in refs. [1–3] we include a number of sub-leading effects, with the aim that we in the end will be able to describe not only the total and diffractive cross sections, but also to generate fully exclusive final states. The main ingredient in our model is energy conservation, which is included by assigning a transverse momentum to each emitted gluon given by the maximum inverse size of the neighboring dipoles. As a result this also implies that the singularities for small dipoles are avoided. Other features are saturation effects in the evolution through a dipole swing mechanism, and a consistent treatment of confinement and running coupling effects in both dipole emissions and dipole–dipole interactions.

Taken together with a very simple model for the initial proton wavefunction, these features allow us to obtain a Lorentz-frame independent description of total cross sections, both for pp and DIS, using basically only two free parameters, a confinement scale $r_{\max}$ and Λ_{QCD} [3]. The model gives a good description of measurements of the total and diffractive cross sections in pp and $\gamma^* p$ collisions, and also for the elastic cross section in pp. In this paper we will continue our investigations with an analysis of exclusive production of vector mesons and real photons in $\gamma^* p$. The aim is to further test our model, and in particular to study the effect of the fluctuations in the cascade. We also extend the analyses to include the t-dependence of the (quasi-)elastic cross sections, including also elastic pp scattering, which in particular gives information about the properties of the incoming proton state.

In the eikonal approximation the quasi-elastic $\gamma^* p$ collisions contain three elements: the virtual photon–dipole vertex, the dipole–proton scattering amplitude, and the vertex for the transition between the dipole and the final vector meson or real photon. Here the first component can be calculated perturbatively, although a hadronic component must be included at lower Q^2-values. In an extensive study Forshaw *et al.* [9,10] have analyzed the results obtained from a set of models for the dipole–proton scattering and for the vector meson wavefunctions, and compared them with experimental data. In this paper we want to carry out a similar analysis, but now use our dipole cascade model for the dipole–proton scattering. We are here particularly interested in effects of fluctuations in the cascade evolution, which are not included in the analyses by Forshaw *et al.* We also want to use this study to put constraints on the state of the incoming proton.

We begin in section 2 with discussing the eikonal formalism for exclusive vector meson production, whereafter we describe our model for dipole evolution and dipole–dipole scattering in section 3 and the models we use for the proton, photon and vector meson wavefunctions in section 4. In section 5 we retune the parameters of our model to data on total and elastic pp cross sections and the total $\gamma^\star p$ cross section before we present our results on quasi-elastic $\gamma^\star p$ cross sections on section 6. Finally we present our conclusions in section 7

2. Formalism

2.1 The dipole cascade model and the eikonal approximation

As discussed in the introduction, our model for pp collisions and DIS is an extension of Mueller's dipole cascade model [4–6]. In this formalism the probability per unit rapidity Y that a dipole $(\boldsymbol{x}, \boldsymbol{y})$ emits a gluon at transverse position $\boldsymbol{z}$ is given by

$$\frac{d\mathcal{P}}{dY} = \frac{\bar{\alpha}}{2\pi} d^2\boldsymbol{z} \frac{(\boldsymbol{x}-\boldsymbol{y})^2}{(\boldsymbol{x}-\boldsymbol{z})^2(\boldsymbol{z}-\boldsymbol{y})^2}, \quad \text{with } \bar{\alpha} = \frac{3\alpha_s}{\pi}. \tag{2.1}$$

The evolution of this cascade agrees with the leading order BFKL evolution. As a consequence, the total number of dipoles grows exponentially. This also implies a strong growth for the total cross section which, however, is tamed by taking multiple dipole interactions into account. The scattering probability between two elementary colour dipoles with coordinates $(\boldsymbol{x}_i, \boldsymbol{y}_i)$ and $(\boldsymbol{x}_j, \boldsymbol{y}_j)$ respectively, is given by

$$f_{ij} = f(\boldsymbol{x}_i, \boldsymbol{y}_i | \boldsymbol{x}_j, \boldsymbol{y}_j) = \frac{\alpha_s^2}{8}\left[\log\left(\frac{(\boldsymbol{x}_i-\boldsymbol{y}_j)^2(\boldsymbol{y}_i-\boldsymbol{x}_j)^2}{(\boldsymbol{x}_i-\boldsymbol{x}_j)^2(\boldsymbol{y}_i-\boldsymbol{y}_j)^2}\right)\right]^2. \tag{2.2}$$

Summing over all i and j this can give a large number, but the unitarized interaction probability determined by

$$T(\mathbf{b}) = 1 - e^{-\sum f_{ij}} \equiv 1 - e^{-F} \tag{2.3}$$

will never exceed 1.

We note that the splitting probability in eq. (2.1) is singular for small dipole sizes $\boldsymbol{x}-\boldsymbol{z}$ or $\boldsymbol{z}-\boldsymbol{y}$, but these small dipoles have a small probability to interact with the target, and the eikonal $F = \sum f_{ij}$ is finite.

In the model developed in refs. [1–3], we extended Mueller's cascade model to include sub-leading effects from energy conservation and a running coupling, saturation effects not only in the dipole–dipole subcollisions but also within the individual cascades, and effects of confinement. These features are further discussed in sec. 3.

The model is supplemented by a non-perturbative model for an initial proton in terms of three dipoles. In the eikonal approximation the total and the diffractive (including the elastic) cross sections are then given by

$$\sigma_{\text{tot}} = 2\int d^2b\,\langle(1-e^{-F})\rangle, \quad \sigma_{\text{diff}} = \int d^2b\,\langle(1-e^{-F})^2\rangle. \tag{2.4}$$

The diffractive cross section can be separated in elastic scattering and diffractive excitation:

$$\sigma_{\text{el}} = \int d^2b\,(\langle 1-e^{-F}\rangle)^2, \quad \sigma_{\text{diff exc}} = \int d^2b\,\left\{\langle(1-e^{-F})^2\rangle - (\langle 1-e^{-F}\rangle)^2\right\}. \tag{2.5}$$

Thus the separation between elastic and inelastic diffraction is determined by the fluctuations in the scattering amplitude. The average in eqs. (2.4) and (2.5) is taken over the different incoming dipole configurations and different cascade evolutions, which thus give two separate sources for fluctuations. The differential cross section $d\sigma_{\text{el}}/dt$ is obtained from the Fourier transform of the scattering amplitude

$$\frac{d\sigma_\lambda}{dt} = \frac{1}{4\pi}\left|\int d^2\mathbf{b}\,e^{i\mathbf{qb}}\langle 1-e^{-F}\rangle\right|^2, \quad \text{with } t=-\mathbf{q}^2. \tag{2.6}$$

2.2 DVCS and exclusive vector meson production in $\gamma^* p$ collisions

We want to study the exclusive processes

$$\gamma^*\,p \to V\,p, \quad V=\gamma,\rho,\psi,\ldots \tag{2.7}$$

In the dipole model the virtual photon is split into a $q\bar{q}$ pair long before the collision. This dipole scatters elastically against the proton, and after the scattering the pair joins again forming a real photon or a vector meson. The formulation in the transverse coordinate plane makes it easier to study these pseudo-elastic reactions, and in the eikonal approximation the scattering amplitude is expressed in terms of three components:

$$\Im A_\lambda(s,\mathbf{b}) = s\sum_{f,h,\bar{h}}\int\int dz\,d^2\mathbf{r}\,\Psi^{*V\lambda}_{fh\bar{h}}(\mathbf{r},z)\,\Psi^{\gamma\lambda}_{fh\bar{h}}(\mathbf{r},z,Q^2)\,\hat{\sigma}_{dp}(s,\mathbf{r},\mathbf{b},z). \tag{2.8}$$

Here $\mathbf{r}$ is the transverse size of the dipole, z and $1-z$ the fractions of the photon or vector meson carried by the quark and antiquark respectively, and h and $\bar{h}$ their helicities. λ denotes the photon or vector meson helicity, $\hat{\sigma}_{dp}$ is the dipole–proton scattering probability with $\mathbf{b}$ the impact parameter, and s the total energy squared.

Neglecting the small contribution from the real part of the amplitude, the total cross section is given by

$$\sigma_\lambda(\gamma^* p\to Vp) = \frac{1}{4s^2}\int d^2\mathbf{b}\,|A_\lambda(s,\mathbf{b})|^2. \tag{2.9}$$

In analogy with eq. (2.6) the differential cross section is obtained from the Fourier transform:

$$\frac{d\sigma_\lambda}{dt} = \frac{1}{16\pi s^2}\left|\int d^2\mathbf{b}\,e^{i\mathbf{qb}}A_\lambda(s,\mathbf{b})\right|^2, \quad \text{with } t=-\mathbf{q}^2. \tag{2.10}$$

3. The improved dipole cascade

As discussed in the introduction, the model developed in refs. [1–3]. is an extension of Mueller's dipole cascade model, which includes sub-leading effects from energy conservation and a running coupling, saturation effects not only in the dipole–dipole subcollisions but also within the individual cascades, and effects of confinement. As mentioned above, an essential point is here that we include the effect of fluctuations in the dipole cascades in the calculation of the elastic or quasi-elastic cross sections.

3.1 Non-leading perturbative effects

3.1.1 Energy-momentum conservation

It is known that the large NLO corrections to the BFKL evolution are reduced significantly if proper energy conservation is included in the leading order. In our model a small transverse extension is interpreted as a large transverse momentum. This interpretation is supported by the resulting analogies between the dipole chains in coordinate space and the chains in the LDC model, which is formulated in momentum space and interpolates smoothly between DGLAP and BFKL evolution. Taking energy-momentum conservation into account is most easily done in a Monte Carlo (MC) simulation. Conserving both light-cone components, p_+ and p_-, implies that we also satisfy the so called consistency constraint [11]. As small dipoles in our formalism correspond to large transverse momenta, energy conservation also gives a dynamical cutoff for the otherwise diverging number of small dipoles, and thus makes the MC simulation much more efficient.

3.1.2 Running coupling

In our simulations we also include non-leading effects from the running of α_{s}, both in the dipole splitting and in the dipole–dipole scattering probability. In the dipole emissions the scale in the coupling is given by $\min(r, r_1, r_2)$, where r is the size of the mother dipole which splits into r_1 and r_2. This is the most natural choice and is also consistent with recent NLO calculations [12–14]. For the dipole–dipole scattering the situation is somewhat more complicated with basically six different dipole sizes involved. We have chosen to use the scale $\min(|\boldsymbol{x}_i - \boldsymbol{y}_i|, |\boldsymbol{x}_j - \boldsymbol{y}_j|, |\boldsymbol{x}_i - \boldsymbol{y}_j|, |\boldsymbol{y}_i - \boldsymbol{x}_j|)$. In order to avoid divergencies the coupling is in all cases frozen so that $\alpha_{\mathrm{s}}(r) \to \alpha_{\mathrm{s}}(\min(r, r_{\max}))$, where $r_{\max}$ is the confining scale discussed in section 3.3 below.

3.2 Saturation within the cascades

Mueller's cascade includes saturation effects from multiple collisions in the Lorentz frame chosen for the calculation, but not saturation effects from gluon interaction within the individual cascades. The result is therefore dependent on the chosen Lorentz frame. In ref. [2] we improved our model by allowing (colour suppressed) recouplings of the dipole chain during the evolution, a "dipole swing". The swing is a process in which two dipoles $(\boldsymbol{x}_i, \boldsymbol{y}_i)$ and $(\boldsymbol{x}_j, \boldsymbol{y}_j)$ are replaced by two new dipoles $(\boldsymbol{x}_i, \boldsymbol{y}_j)$ and $(\boldsymbol{x}_j, \boldsymbol{y}_i)$. The process can be interpreted in two ways. There is a probability $1/N_c^2$ that the two dipoles may have the same colour, and the quark at $\boldsymbol{x}_i$ and the antiquark at $\boldsymbol{y}_j$ form a colour singlet.

In this case the best approximation of the quadrupole field ought to be obtained by the closest charge-anticharge combinations. Here the swing is therefore naturally suppressed by $1/N_c^2$, and it should be more likely to replace two given dipoles with two smaller ones. Secondly, we may see it as the result of a gluon exchange between the dipoles, which results in a change in the colour flow. In this case the swing would be proportional to α_s^2, which again is formally suppressed by N_c^2, compared to the splitting process in eq. (2.1), which is proportional to $\bar{\alpha} = N_c\alpha_s/\pi$.

In the MC implementation each dipole is randomly given one of N_c^2 possible colour indices. Only dipoles with the same colour can swing, and the weight for a swing $(\boldsymbol{x}_1, \boldsymbol{y}_1), (\boldsymbol{x}_2, \boldsymbol{y}_2) \to (\boldsymbol{x}_1, \boldsymbol{y}_2), (\boldsymbol{x}_2, \boldsymbol{y}_1)$ is determined by a factor proportional to

$$\frac{(\boldsymbol{x}_1 - \boldsymbol{y}_1)^2(\boldsymbol{x}_2 - \boldsymbol{y}_2)^2}{(\boldsymbol{x}_1 - \boldsymbol{y}_2)^2(\boldsymbol{x}_2 - \boldsymbol{y}_1)^2}. \tag{3.1}$$

This implies that the swing favors the formation of smaller dipoles. The number of dipoles is not reduced by the swing, but the fact that smaller dipoles have smaller cross sections gives the desired suppression of the total cross section. Although not explicitely frame independent the results from the MC simulations are very nearly independent of the Lorentz frame used for the calculations.

3.3 Confinement effects

Mueller's dipole model is a purely perturbative process. It should therefore be applied to small dipoles, *e.g.* to heavy quarkonium states. When applying the dipole formalism to collisions with protons it is necessary to take confinement into account, in order to prevent the formation of very large dipoles. Confinement effects must also suppress long range interactions between colliding dipoles. In ref. [3] a consistent treatment of confinement was presented by replacing the Coulomb potentials in eqs. (2.2) and (3.3) by screened potentials, with a screening length $r_{\max}$.

Obviously the dipoles produced in the splitting process in eq. (2.1) cannot become too large, and it is natural to introduce a scale $r_{\max}$, so that larger dipoles are suppressed. In a similar way confinement must suppress long range interactions between colliding dipoles.

The formula for f_{ij} in eq. (2.2) is just the two dimensional Coulomb potential, and can be written as

$$f(\boldsymbol{x}_i, \boldsymbol{y}_i|\boldsymbol{x}_j, \boldsymbol{y}_j) = \frac{g^4}{8}[\Delta(\boldsymbol{x}_i - \boldsymbol{x}_j) - \Delta(\boldsymbol{x}_i - \boldsymbol{y}_j) - \Delta(\boldsymbol{y}_i - \boldsymbol{x}_j) + \Delta(\boldsymbol{y}_i - \boldsymbol{y}_j)]^2 \tag{3.2}$$

where $\Delta(\boldsymbol{r})$ is the Green's function given by

$$\Delta(\boldsymbol{r}) = \int \frac{d^2\boldsymbol{k}}{(2\pi)^2} \frac{e^{i\boldsymbol{k}\cdot\boldsymbol{r}}}{\boldsymbol{k}^2}. \tag{3.3}$$

To take confinement into account we replace the infinite range Coulomb potential with a screened Yukawa potential. This implies that the Coulomb propagator $1/\boldsymbol{k}^2$ in eq. (3.3) is replaced by $1/(\boldsymbol{k}^2 + M^2)$, where $M = 1/r_{\max}$ is the confinement scale. As a result, the four functions Δ in eq. (3.2) will be replaced by

$$\int \frac{d^2\boldsymbol{k}}{(2\pi)^2} \frac{e^{i\boldsymbol{k}\cdot\boldsymbol{r}}}{\boldsymbol{k}^2 + 1/r_{\mathrm{max}}^2} = \frac{1}{2\pi} K_0(r/r_{\mathrm{max}}) \tag{3.4}$$

with K_0 a modified Bessel function. For small separations, where $r \ll r_{\mathrm{max}}$, the function $K_0(r/r_{\mathrm{max}})$ behaves like $\ln(r_{\mathrm{max}}/r)$, and we then recognize the result in eq. (2.2). For large separations, $r \gg r_{\mathrm{max}}$, $K_0(r/r_{\mathrm{max}})$ falls off exponentially $\sim \sqrt{\frac{\pi r_{\mathrm{max}}}{r}} e^{-r/r_{\mathrm{max}}}$, as expected from confinement.

In a similar way, the underlying Coulomb potential in the dipole splitting function in eq. (2.1) can be replaced by a screened Yukawa potential, using again the replacement $1/\boldsymbol{k}^2 \to 1/(\boldsymbol{k}^2 + 1/r_{\mathrm{max}}^2)$. The modified splitting probability is then given by

$$\frac{d\mathcal{P}}{dY} \to \frac{\bar{\alpha}}{2\pi} d^2\boldsymbol{z} \left\{ \frac{1}{r_{\mathrm{max}}} \frac{\boldsymbol{x}-\boldsymbol{z}}{|\boldsymbol{x}-\boldsymbol{z}|} K_1\left(\frac{|\boldsymbol{x}-\boldsymbol{z}|}{r_{\mathrm{max}}}\right) - \frac{1}{r_{\mathrm{max}}} \frac{\boldsymbol{y}-\boldsymbol{z}}{|\boldsymbol{y}-\boldsymbol{z}|} K_1\left(\frac{|\boldsymbol{y}-\boldsymbol{z}|}{r_{\mathrm{max}}}\right) \right\}^2. \tag{3.5}$$

For small arguments $K_1(r/r_{\mathrm{max}}) \approx r_{\mathrm{max}}/r$, from which we get back the result in eq. (2.1), while for large arguments $K_1(r/r_{\mathrm{max}}) \sim \sqrt{\pi r_{\mathrm{max}}/r} \cdot e^{-r/r_{\mathrm{max}}}$, and once again we obtain an exponentially decaying field.

4. Initial wave functions

4.1 Proton wave function

In ref. [2] we also introduced a simple model for the proton in terms of three dipoles with extensions determined by a Gaussian distribution. The resulting model was in good agreement with total cross sections for both DIS and pp collisions. It was shown in [15] that the three valence quarks in a proton emits gluons in transverse space with the same distribution as three dipoles, only with half the intensity. Thus, by modeling the proton with a closed chain of three gluons we emulate the fact that a proton at rest may contain more charges than its valence quarks. This is analogous to the finding of Glück, Reya and Vogt, who needed a large valence-like gluon component when trying to fit parton densities evolved from a very low scale [16]. Thus, although not a fully realistic description of the initial non-perturbative proton state, the model appears to give a fair representation of the multi-dipole system obtained at the low x-values, which are important for the high energy collisions.

The results turned out to be almost independent of the shape of the three starting gluons, except for the size of the triangle. In fact, equilateral triangles that were allowed to vary in only size and orientation turned out to model the proton as well as more complicated formations. With a Gaussian distribution for the size of equilateral triangles, motivated by the exponential dependence on t for the elastic cross section, data on total cross sections for DIS and pp collisions are well reproduced, when the width of the Gaussian was tuned to 3.5 GeV$^{-1} \approx 0.66$ fm.

As discussed above, the differential and elastic cross sections are determined by the fluctuations in the scattering amplitude, and in ref. [3] it was pointed out that a Gaussian wavefunction as discussed above must overestimate the fluctuations of the incoming state in its rest frame. The probability for the three quarks to simultaneously be located in a single point ought to be suppressed, and it was emphasized that the exponential t-dependence of the elastic cross section, which motivated the Gaussian shape, is only observed for $|t| < 0.15\,\mathrm{GeV}^2$, corresponding to $b \gtrsim 1$ fm. A wavefunction of the form

$$|\Psi|^2 = C\, e^{-(r-R_p)^2/w^2} \tag{4.1}$$

was also tested, and found to give essentially identical total cross sections. The fluctuations are here suppressed by a small value of w, and in ref. [3] it was observed that reducing the fluctuations to a minimum gave good agreement with the integrated elastic and diffractive cross sections in pp collisions. Lacking further constraints we could, however, only present an upper limit for σ_{el}, by neglecting the fluctuations in the wavefunction, thus including only those in the cascade evolution.

An essential motivation for the present analysis of quasi-elastic $\gamma^* p$ cross sections and of the t-dependence of the pp elastic cross section, is to check whether the fluctuations in the dipole cascade model are also consistent with these observables, and if more constraints can be put on the shape of the initial proton state. In this analysis we will use the two-parameter form in eq. (4.1), and see if this can be adjusted to reproduce also the (quasi-)elastic cross sections.

At this point we also note that in many analyses the fluctuations in the cascade evolution are neglected. This means that e^{-F} is replaced by $e^{-<F>}$ in eqs. (2.4) and (2.5). Including also the fluctuations in the cascade implies that the impact parameter profile has to be more "gray" and less "black and white". As an example the amplitude $\langle T(b=0)\rangle$ is a factor 2/3 smaller in our formalism than in the analysis by Kowalski and Teaney [17], for a dipole of size $2\,\mathrm{GeV}^{-1}$ and $x = 10^{-4} - 10^{-5}$.

4.2 Photon wavefunction

4.2.1 Large Q^2

For large Q^2 the coupling of the γ^* to the $q\bar{q}$ pair can be calculated perturbatively. The well known result to leading order is

$$\begin{aligned}
\Psi^{\gamma 0}_{fh\bar{h}}(Q,r,z) &= \frac{\sqrt{\alpha_{EM}N_C}}{\pi} Qz(1-z)e_f K_0(r\varepsilon_f)\delta_{h\bar{h}} \\
\Psi^{\gamma +}_{fh\bar{h}}(Q,r,z) &= \frac{\sqrt{\alpha_{EM}N_C/2}}{\pi} e_f\Big(ie^{i\theta}\left(z\delta_{h+}\delta_{\bar{h}-} - (1-z)\delta_{h-}\delta_{\bar{h}+}\right)\varepsilon_f K_1(r\varepsilon_f) + \\
&\qquad\qquad +\delta_{h+}\delta_{\bar{h}+} m_f K_0(r\varepsilon_f)\Big)
\end{aligned} \tag{4.2}$$

with

$$\varepsilon_f = \sqrt{z(1-z)Q^2 + m_f^2}. \tag{4.3}$$

Here $\lambda = 0$ and $+$ denote the longitudinal and transverse wavefunctions respectively, f denotes the quark flavour, and K_0 and K_1 are modified Bessel functions. e_f is the electric charge of the quark in units of the proton charge and m_f the effective mass of the quark.

4.2.2 Smaller Q^2

For smaller Q^2 the photon has also a hadronic component. In [18] it was shown that also the total $\gamma^\star p$ cross section at HERA could be well described over a wide range of energies and virtualities, when the hadronic component was simulated by a relatively small effective quark mass ≈ 60 MeV. For the exclusive reactions studied here we need a more careful treatment of the hadronic component, and we expect that these processes can provide relevant constraints on the photon wavefunction. The hadronic component should be particularly important for the real photons produced in Deeply virtual Compton scattering (DVCS).

For small Q^2 a small effective quark mass allows for rather large dipoles with a corresponding large cross section. In the present analysis we include an improved description of confinement effects in the dipole evolution (see section 3.3), and we will therefore try to include confinement effects also in the photon wavefunction. Our photon model is inspired by the Vector Meson Dominance modeling introduced by Forshaw *et al.* in [9] (which, in turn, was inspired by [19]). This model contains an enhancement factor for dipoles of a typical hadronic size, together with a large quark mass which suppresses dipoles larger than the confinement scale. In our model we will use the same enhancement factor, but we use a suppression of large dipoles related to the confinement scale $r_{\max}$, instead of the large quark mass used in ref. [9].

The actual implementation in our MC program relies on shrinking dipoles larger than $r_{\max}$ by reducing the size r_{pert} generated according to the perturbative photon wavefunction to r_{soft}, defined by

$$r_{\text{soft}}(r_{\text{pert}}) = R_{\text{shrink}}\sqrt{\ln\left(1+\frac{r_{\text{pert}}^2}{R_{\text{shrink}}^2}\right)}. \tag{4.4}$$

For small dipoles this gives $r_{\text{soft}} \approx r_{\text{pert}}$, but for large dipoles it gives a Gaussian suppression. The parameter R_{shrink} is adjusted to give the same effective cutoff, $r_{\max}$, as the one obtained for large dipoles in the cascade evolution. This is obtained for $R_{\text{shrink}} = 4.3\,\text{GeV}^{-1}$.

The enhancement factor for dipoles with a typical hadronic size, introduced in ref. [9], is given by the form

$$f(r) = \frac{1+B_V\exp(-(r-R_V)^2/w_V^2)}{1+B_V\exp(-R_V^2/w_V^2)} \tag{4.5}$$

This factor multiplies the squared photon wavefunction after the shift in eq. (4.4). The enhancement resembles very much the shape we use for the proton wavefunction in eq. (4.1), and we can think of the the whole correction

$$|\Psi_\gamma(r_{\text{pert}})|^2 \to |\Psi_\gamma(r_{\text{soft}})|^2\, f(r_{\text{soft}}) \tag{4.6}$$

as the modeling of the virtual photon fluctuating into vector meson states with r-values of a hadronic scale. Partly this enhancement can be thought of as due to a longer lifetime of these states, and partly a simulation of a gluonic component in the vector meson, in a way similar to our model of the initial proton wavefunction in section 4.1. The photon model contains three adjustable parameters, B_V, R_V, and w_V, which have to be determined from experiments.

	Boosted Gaussian			
V	M_V	m_{uds}	m_c	R^2
ρ	0.77	0.06	1.4	12.3
ϕ	1.02	0.06	1.4	2.44
ψ	3.1	0.06	1.4	10

	DGKP				
V	M_V	m_{uds}	m_c	ω_L	ω_T
ρ	0.77	0.06	1.4	0.33	0.22
ϕ	1.02	0.06	1.4	0.37	0.26
ψ	3.1	0.06	1.4	0.69	0.56

Table 1: The parameters used for the boosted Gaussian and DGKP wavefunctions in this paper in GeV-based units.

4.3 Meson wavefunctions

The wavefunction of a vector meson cannot be calculated perturbatively, and has to be described by models. In the rest frame it is generally assumed that the lowest Fock state with a single $q\bar{q}$ pair dominates. This component must then be normalized to 1, in contrast to the photon for which the $q\bar{q}$ state is a perturbative fluctuation. In addition the wavefunction at the origin is determined by the decay rate of the vector meson. Thus there are two constraints allowing two parameters in an ansatz to be determined. In a boosted frame higher Fock states may then be generated by gluon emission. Different models can differ in the functional form used for the wavefunction in the rest frame, and in the description of the transition from coordinate space to the momentum fractions z and $1-z$ used in the light-cone wavefunction. We will here concentrate on the DGKP model [20] and the boosted Gaussian model [9], which in the analysis by Forshaw *et al.* give the best agreement with the experimental data.

4.3.1 The DGKP model

In this model for the meson wavefunction, proposed by Dosch, Gousset, Kulzinger, and Pirner [20], it is assumed that the dependence on the transverse and longitudinal coordinates, r and z, factorizes. The transverse part of the wavefunction is assumed to be a pure Gaussian, consistent with soft hadron–hadron collisions. For the longitudinal component it assumes the form proposed by Wirbel, Stech and Bauer [21]. The resulting light-cone wavefunction has the following form:

$$
\begin{aligned}
\Psi^{V0}_{fh\bar{h}}(r,z) &= \mathscr{N}_0 M_V \delta_{-h\bar{h}} z(1-z)\sqrt{z(1-z)}\exp\left(-\frac{r^2\omega_L^2}{2}\right)\exp\left(-\frac{M_V^2(z-0.5)^2}{2\omega_L^2}\right) \\
\Psi^{V+}_{fh\bar{h}}(r,z) &= \mathscr{N}_+\left(\omega_T^2 rie^{i\theta}(z\delta_{h+}\delta_{\bar{h}-}-(1-z)\delta_{h-}\delta_{\bar{h}+})+m_f\right)\sqrt{z(1-z)}\times \\
&\qquad \exp\left(-\frac{M_V^2(z-0.5)^2}{2\omega_T^2}\right)\exp\left(-\frac{r^2\omega_T^2}{2}\right).
\end{aligned}
\tag{4.7}
$$

Here M_V is the mass of the vector meson, and the size parameter ω and the normalization constant $\mathscr{N}$ are determined from the electronic decay rate and the normalization condition. (Our notation differs from the original paper, as we have collected the multiplicative factors in the normalization constant $\mathscr{N}$.) The shape of the wavefunction of the ρ with the parameters we have used (see table 1) can be seen in figure 1.

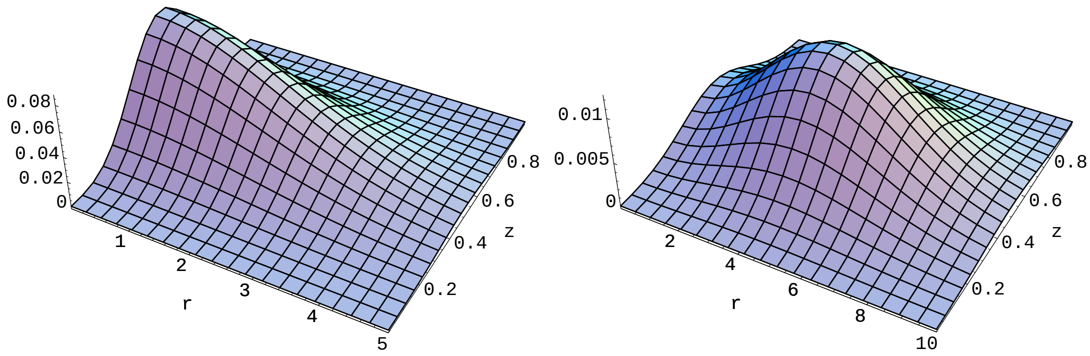

Figure 1: The wavefunctions $|\Psi_L(r,z)|^2$ (left) and $|\Psi_T(r,z)|^2$ (right) of the DGKP model for a ρ meson with our quark mass of 60 MeV. Note the different scales in r, both in GeV^{-1}.

4.3.2 The boosted Gaussian model

The "boosted" models are obtained by assuming a given wavefunction in the meson rest frame. This is then boosted into a light-cone wavefunction using the Brodsky-Huang-Lepage prescription [22], in which the invariant mass of the quark-antiquark pair is the same in the rest frame and the light-cone frames. The result of this procedure is not factorizing in r and z. In the simplest version the initial wavefunction in the rest frame is a simple Gaussian. In an alternative version by Nemchik *et al.* [23] a hard Coulomb contribution is added, dominating for small r. For the pure Gaussian version suggested by Forshaw *et al.*, which we assume in this analysis, the resulting wavefunction has the following form

$$\begin{aligned}
\Psi^{V0}_{fh\bar{h}}(r,z) &= \frac{\mathcal{N}_0}{M_V}\left(z(1-z)M_V^2 + m_f^2 + 8\frac{z(1-z)}{R^2} - \left(4\frac{z(1-z)r}{R^2}\right)^2\right)\delta_{h\bar{h}}\times \\
&\qquad \exp\left(-\frac{m_f^2R^2}{8z(1-z)}\right)\exp\left(-2z(1-z)\frac{r^2}{R^2}\right)\exp\left(\frac{R^2}{2}m_f^2\right) \qquad (4.8)\\
\Psi^{V+}_{fh\bar{h}}(r,z) &= \mathcal{N}_+\left(4z(1-z)\frac{r}{R^2}ie^{i\theta}(z\delta_{h+}\delta_{\bar{h}-} - (1-z)\delta_{h-}\delta_{\bar{h}+}) + m_f\delta_{h+}\delta_{\bar{h}+}\right)\times \\
&\qquad \exp\left(-\frac{m_f^2R^2}{8z(1-z)}\right)\exp\left(-2z(1-z)\frac{r^2}{R^2}\right)\exp\left(\frac{R^2}{2}m_f^2\right)
\end{aligned}$$

In this model the transverse size R of the meson, and the normalization $\mathcal{N}_\lambda$ are the two parameters to be tuned. (In our notation all multiplicative constants have also here been included in a single normalization constant.) The shape of the wavefunction for the ρ meson using the parameters in table 1 is shown in figure 2.

5. Tuning of parameters and the differential *pp* cross section

5.1 The total and elastic *pp* cross section

We start by tuning the model to *pp* scattering data. Here the model contains 4 parameters,

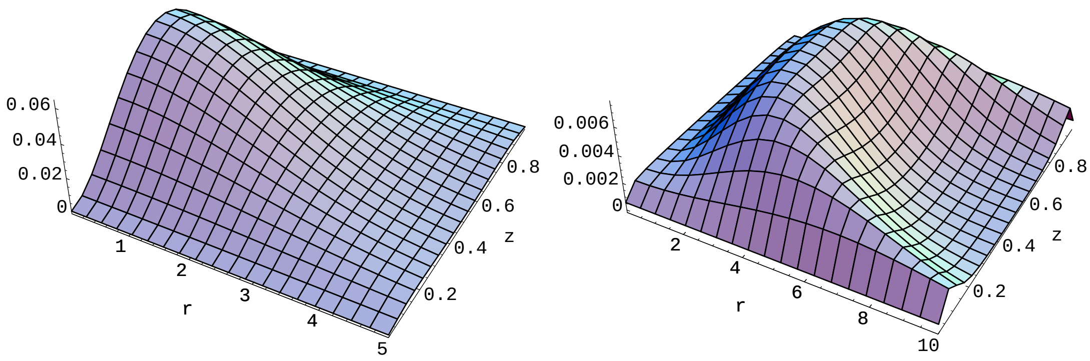

Figure 2: The wavefunctions $|\Psi_L(r,z)|^2$ (left) and $|\Psi_T(r,z)|^2$ (right) of the Boosted Gaussian model for a ρ meson with our quark mass of 60 MeV. Note the different scales in r, both in GeV^{-1}.

$\Lambda_{\rm QCD}$ and $r_{\rm max}$ describing the dipole evolution, and R_p and w determining the proton wave function in eq. (4.1) (with C fixed by normalization). In ref. [3] we found that the values for $\Lambda_{\rm QCD}$ and $r_{\rm max}$ are correlated, such that a larger $r_{\rm max}$ can be compensated by a smaller $\Lambda_{\rm QCD}$. It was also noted that the integrated elastic cross section favors a narrow proton wave function, corresponding to a small value for the parameter w. A large w-value, or a single Gaussian $\propto \exp(-\mathbf{r}^2/R_p^2)$, gives too large fluctuations and correspondingly a too small elastic cross section. To constrain the fit we here add the differential cross section $d\sigma/dt$ to the integrated cross sections $\sigma_{\rm tot}$, $\sigma_{\rm diff}$, and $\sigma_{\rm el}$ studied in [3]. We will then in next section check if the result also can reproduce the quasi-elastic cross sections in $\gamma^* p$ collisions.

With the proton wavefunction given by eq. (4.1) the total and elastic cross sections are given by

$$\sigma_{\rm tot} = 2\int d^2\mathbf{b} d^2\mathbf{r}_{p1} d^2\mathbf{r}_{p2}\, |\Psi_p(\mathbf{r}_{p1})|^2\, |\Psi_p(\mathbf{r}_{p2})|^2\, \langle 1-e^{-F}\rangle_{12}, \tag{5.1}$$

$$\sigma_{\rm el} = \int d^2\mathbf{b} \left| \int d^2\mathbf{r}_{p1} d^2\mathbf{r}_{p2}\, |\Psi_p(\mathbf{r}_{p1})|^2\, |\Psi_p(\mathbf{r}_{p2})|^2\, \langle 1-e^{-F}\rangle_{12} \right|^2. \tag{5.2}$$

Here $\mathbf{b}$ is the impact parameter, $\mathbf{r}_{pi}$ ($i=1,2$) parameterizes the size and orientation of the triangles describing the colliding protons. The Monte Carlo is used to simulate the dipole evolution in the rest frame of the collision, and to calculate $1-e^{-F}$. The average $\langle 1-e^{-F}\rangle_{12}$ is over simulations for fixed impact parameter and starting dipole states $\mathbf{r}_1$ and $\mathbf{r}_2$. Note that in the elastic cross section the average over evolutions and the integrals over the wave functions is taken on amplitude level before taking the absolute square.

When tuning the parameters we find that all observables are almost independent of w below 0.5 GeV^{-1}. We therefore decided to neglect the fluctuations in the proton size completely and set the width to zero, turning the proton wavefunction into a delta function at R_p.

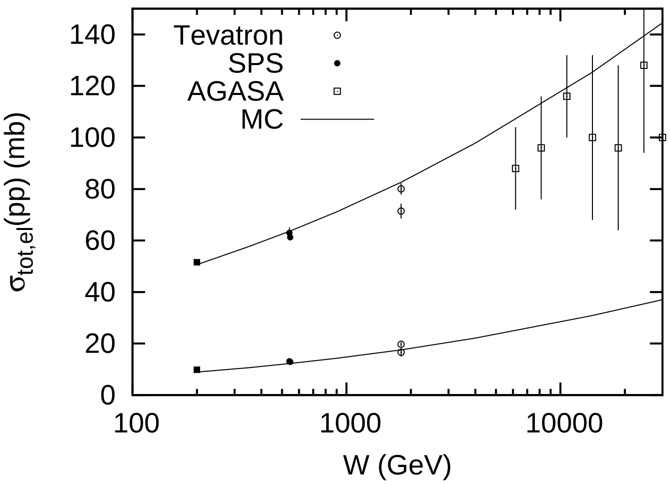

Figure 3: The total and elastic cross section for pp collision. The upper cross sections are total cross sections, while the lower cross sections are the elastic ones. Tevatron data are from [24–27], SPS data are from [28] and cosmic ray data are from [29]. The lines are our model with tuned parameters.

If the total and integrated elastic cross sections are tuned at one energy, we find that the energy dependence of these cross sections depends very weakly, if at all, on the parameters of the model. Thus this energy dependence cannot be tuned, and the fact that it is close to the experimental results is therefore a direct consequence of the model. Our results for the total and elastic pp cross sections can be seen in figure 3.

Extrapolating to higher energies we find the total cross section at the LHC nominal energy, 14 TeV, to be about 125 mb (117 mb at 10 TeV). We note that this is a rather high value compared to other predictions. Thus the Donnachie-Landshoff parameterization gives 101.5 mb at 14 TeV [30], while an analysis by Khoze, Martin, and Ryskin gives about 90 mb [31]. The predicted elastic cross section is about 31 mb for the LHC at 14 TeV (28 mb at 10 TeV).

5.2 The differential elastic pp cross section

The differential elastic pp cross section is given by

$$\frac{\sigma_{\mathrm{el}}}{dt} = \frac{1}{4\pi}\left|\int d^2\mathbf{b}e^{-i\mathbf{q}\cdot\mathbf{b}}d^2\mathbf{r}_{p1}d^2\mathbf{r}_{p2}\left|\Psi_p(\mathbf{r}_{p1})\right|^2\left|\Psi_p(\mathbf{r}_{p2})\right|^2\langle 1-e^{-F}\rangle_{12}\right|^2, \text{ with } t=-\mathbf{q}^2. \tag{5.3}$$

We here neglect the real part of the amplitude, and therefore $d\sigma/dt$ will have zeroes from the Fourier transform of the amplitude in eq. (5.3). Even though the true complex amplitude will not be identically zero, the real part is still assumed to be small, producing a dip at some value $t = t_0$, related to the inverse square of the size of the proton at the relevant energy. This dip is visible in some of the experimental data shown in figure 4, where we have also included the results from the simulations. The parameters which are most sensitive to these distributions are R_p, which determines the size of the proton at rest,

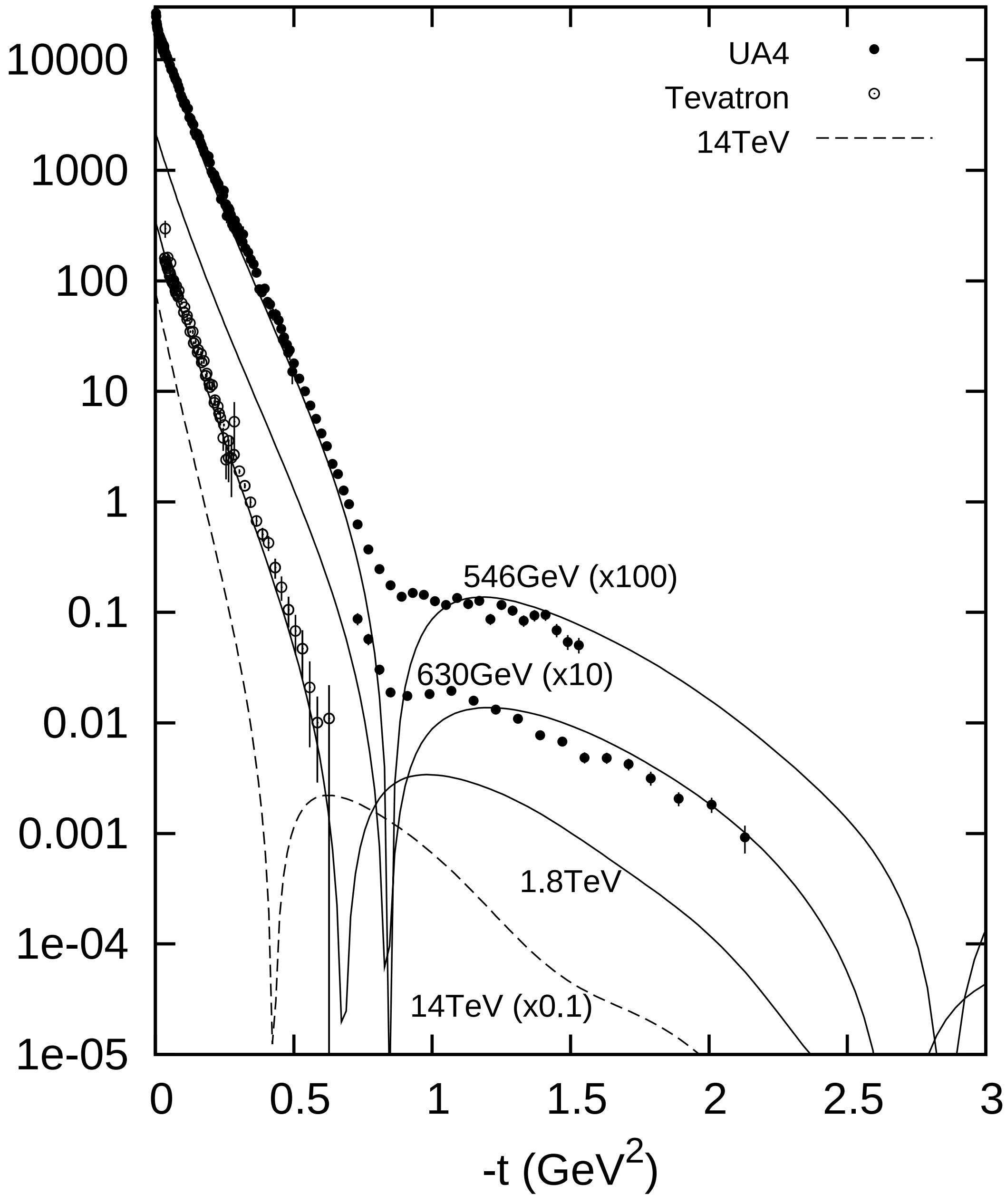

Figure 4: The elastic cross section as function of t in mb/GeV^2. The numbers in parenthesis indicate how the data has been scaled. The lines are our model with tuned parameters. Predictions for 14 TeV is also included. Data are from [24, 32], [33] and [34].

and $r_{\max}$ which regulates the maximal size of new dipoles, and therefore the increase with energy of the proton radius and the variation of the dip position. However, the slope of the distribution is basically independent of our parameters, as is the cross section at large

$\Lambda_{\rm QCD}$	0.2 GeV
$r_{\max}$	2.9 GeV^{-1}
R_p	3.0 GeV^{-1}
w	0 GeV^{-1}

Table 2: The tuned values the parameters for the proton wavefunction and the perturbative evolution used for our model throughout this paper.

t-values. Nevertheless, we are able to get a very good description of the data at all t-values even though the cross sections vary over many orders of magnitude. In figure 4 we also show our result for the LHC, which predicts the location of the dip in the t-dependence at 0.43 GeV^2 at $\sqrt{s} = 14$ TeV (0.47 GeV^2 at 10 TeV). The values of the tuned parameters can be found in table 2.

5.3 The total $\gamma^\star p$ cross section and tuning the photon wave function

We will here use $\Psi_\gamma(Q, \mathbf{r}, z)$ to denote the photon wavefunction in eq. (4.6), where for small Q^2 the perturbative wavefunction is modified to account for the hadronic component of the photon. The total $\gamma^* p$ cross section can be written

$$\sigma_{tot}(\gamma^* p) = \sum_{\lambda f} \int d^2\mathbf{b} d^2\mathbf{r}_p d^2\mathbf{r} dz \, |\Psi_p(\mathbf{r}_p)|^2 \left|\Psi^\lambda_{\gamma,f}(Q,\mathbf{r},z)\right|^2 \langle 1 - e^{-F}\rangle_{dp}, \tag{5.4}$$

where λ is the polarization of the photon and f is the flavour of the quark-antiquark pair created by the photon. $\langle 1 - e^{-F}\rangle_{dp}$ is now an average of the evolution of the dipole from the photon side and of the dipoles from the proton side. It depends not only on the total energy, the size of the proton and photon dipoles and b, but has also a weak dependence on z.

The three parameters B_V, R_V and w_V in the enhancement factor in eq. (4.5) were fitted to the total $\gamma^\star p$ cross section as measured at HERA. Here the value of R_V determines the range in Q^2 where the enhancement is significant, while w_V determines how fast it falls off for large Q^2. The parameter B_V is just an overall strength of the hadronic component.

A good fit to data was obtained with a wave function for the hadronic component similar to the proton wave function, having a size $R_V \approx 3$ GeV^{-1} and a small width. The total $\gamma^\star p$ cross section with and without the effects of confinement and vector meson contributions are shown in figure 5. The tuned values are given in table 3. These parameters are quite different from the ones used by Forshaw *et al.*, who had an R_V of 6.84 GeV^{-1} and a fairly large width [35], which thus gives a stronger enhancement for large dipoles. For large dipole sizes the elementary dipole-proton cross section assumed in ref. [9] are also significantly different from the corresponding ones in our model. The reason why we anyhow can get similar results is that in [9] the very large dipoles are suppressed by a large quark mass, and the enhancement therefore not very effective. A reason for a smaller width in our wavefunction is also that fluctuations in the dipole cascade are included in our formalism, which is compensated by less fluctuations in the wavefunction.

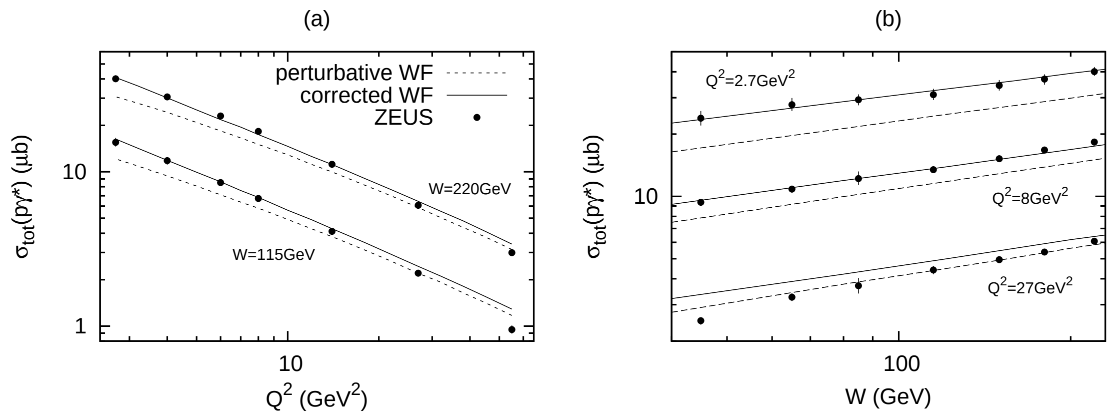

Figure 5: The total cross section of photon–proton collision as function of photon virtuality and center-of-mass energy. The dashed line is calculated with a purely perturbative photon wavefunction, while the full line is with a photon wavefunction with both confinement and VMD corrections. Experimental data are from [36]

R_V	3.0 GeV^{-1}
w_V	0.2 GeV^{-1}
B_V	9.0

Table 3: The tuned values of the parameters of the vector meson resonance function $f(r)$ used for our model throughout this paper.

We also note that the cross sections presented in fig. 5 are somewhat smaller than the corresponding results in refs. [3] and [18]. This is a consequence of the more consistent treatment of confinement in the present analysis, which gives a stronger suppression for larger dipoles. We believe, however, that a much stronger test of the hadronic component will rely on the results for the quasi-elastic reactions discussed in next section.

6. Results for quasi-elastic $\gamma^\star p$ collisions

In this section we will study predictions for quasi-elastic $\gamma^* p$ collisions, using the photon wavefunction parameters determined in section 5.3.

6.1 Deeply Virtual Compton Scattering

In Deeply Virtual Compton Scattering, DVCS, the incoming particle is a virtual photon, while the outgoing particle is a real photon with wavefunction $\Psi^{\lambda}_{\gamma,f}(0,\mathbf{r},z)$. According to eqs. (2.8, 2.9) the cross section is given by

$$\sigma_{\rm DVCS} = \int d^2\mathbf{b} \sum_{\lambda} \left| \int d^2\mathbf{r}_p d^2\mathbf{r} dz \sum_f |\Psi_p(\mathbf{r}_p)|^2 \, \Psi_f^{\star\gamma\lambda}(Q,\mathbf{r},z) \Psi_f^{\gamma\lambda}(0,\mathbf{r},z) \langle 1 - e^{-F} \rangle_{dp} \right|^2 . \tag{6.1}$$

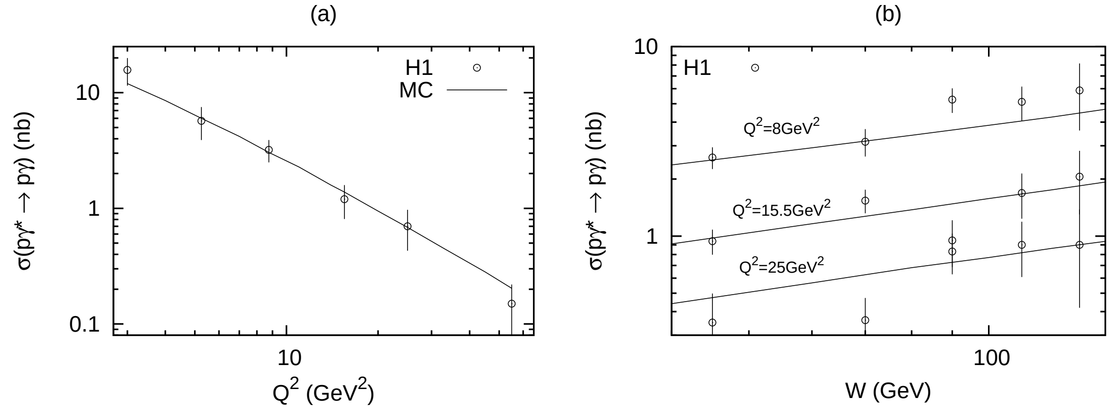

Figure 6: The cross section of $\gamma^\star p \to \gamma p$ for $W = 82$ GeV as function of Q^2 (a) and as function of W for three different Q^2 (b). Experimental data are from [37, 38].

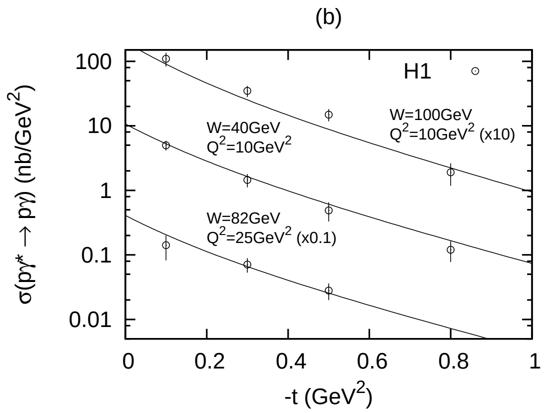

Figure 7: The cross section of $\gamma^\star p \to \gamma p$ as function of t. The brackets refers to (W, Q^2). Note that the three series have been scaled by 10,1 and 0.1 for better readability. Experimental data are from [38].

The differential cross section $d\sigma/dt$ is obtained from the Fourier transform as shown in eq. (2.10). The results obtained using the parameter values in table 3 are presented in figures 6 and 7. We see that the results from the model indeed agrees with the data, both in normalization and in the dependence on Q^2, W and t. As this quasi-elastic reaction is very sensitive to the fluctuations and the transverse size of the hadronic component of the real photon, this is a clear support for the proton-like wave function.

6.2 Exclusive Production of Light vector Mesons

The cross section for exclusive vector meson production, $\gamma^\star p \to Vp$, can be calculated in exactly the same way as for DVCS, only replacing the real photon wavefunction by a meson

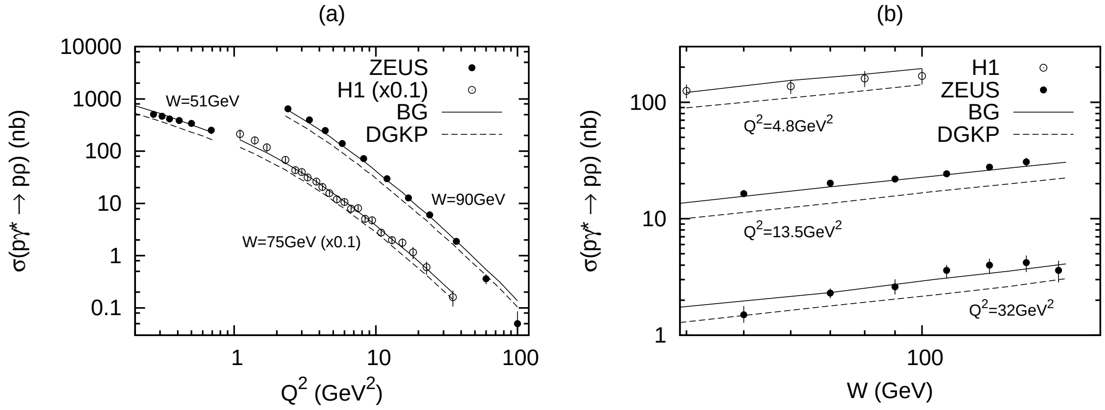

Figure 8: The cross section for $\gamma^\star p \to \rho p$. (a) As function of the photon virtuality. The H1 data has been moved down a factor 10 for better readability. The full and dashed line are with the two different meson wavefunction described in 4.3. (b) As function of the center-of-mass energy W. Experimental data are from [39–41].

wavefunction:

$$\sigma_{\rm el} = \int d^2\mathbf{b} \sum_\lambda \left| \int d^2\mathbf{r} d^2\mathbf{r}_p dz \sum_f |\Psi_p(\mathbf{r}_p)|^2 \, \Psi_f^{\star\gamma\lambda}(Q^2, \mathbf{r}, z) \Psi_f^{V\lambda}(\mathbf{r}, z) \langle 1 - e^{-F} \rangle_{dp} \right|^2 . \quad (6.2)$$

As before we have ignored the real part of the amplitude. Contrary to the case of pp scattering it has been shown in [9] that in exclusive production of light vector mesons the real part can be quite large, for large Q^2 or large W as large as one half of the imaginary part. This would mean that we underestimate the cross section by up to 25% in these regions. However, compared to the uncertainties in the vector meson wavefunctions, this error is small.

From our tuning of the hadronic part of the photon wavefunction, it could seem natural to assume some universal hadron size and maybe try to model the vector meson wavefunctions as a simple gluon–gluon dipole with a size of 3 GeV^{-1} and a small width. However, this would not naturally give us a z-dependence and we would not include the possibility that the vector meson may fluctuate into a photon, which could correspond to an enhancement at small r-values. Therefore we will simply use the boosted Gaussian and DGKP wavefunctions introduced in section 4.3 to estimate the $\gamma^\star p \to Vp$ cross section. Throughout we will use the parameters listed in table 1.

As before, the t-dependence of the cross section can be calculated through a Fourier transform of the amplitude. We are also able to calculate the ratio between the longitudinal to the transverse cross sections and compare with experimental data.

Starting with ρ meson production, the results are shown in figures 8 and 9. We see that the model calculations reproduce experimental data rather well, including the dependence on virtuality Q^2, energy W and momentum transfer t. The Boosted Gaussian wavefunction is in general providing the closer fit, while DGKP is having problems mainly in the ratio

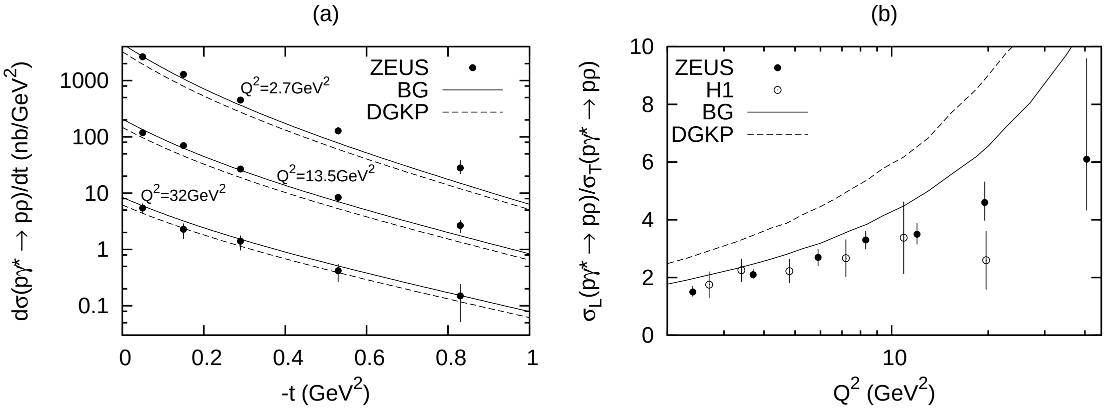

Figure 9: (a) The differential cross section for $\gamma^\star p \to \rho p$ as function of transferred momentum squared $|t|$. Three different Q^2 has been used, all with a center-of-mass energy of 90 GeV. (b) The ratio of longitudinal and transverse cross section for $\gamma^\star p \to \rho p$ as function of the photon virtuality. Experimental data are from [39, 40].

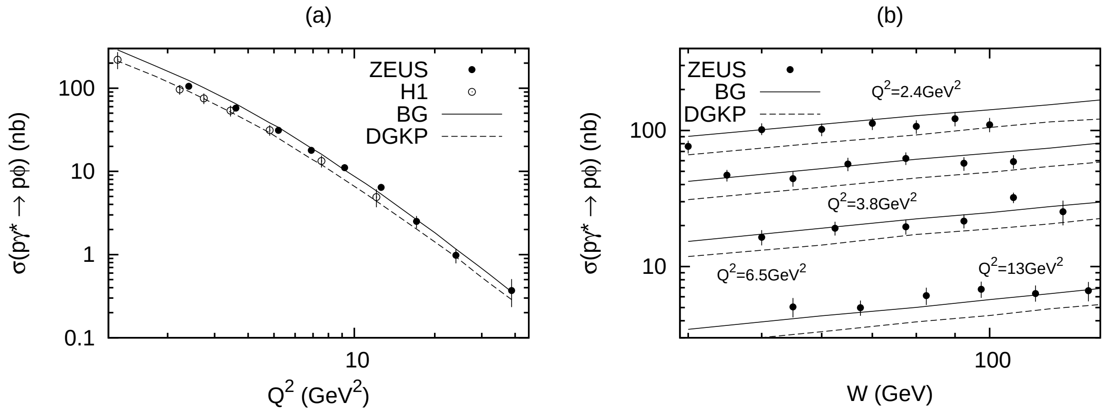

Figure 10: The cross section for $\gamma^\star p \to \phi p$ (a) As function of the photon virtuality at center-of-mass energy 75 GeV. The full and dashed line are with the two different meson wavefunction described in section 4.3. (b) As function of the center-of-mass energy for four different photon virtualities Q^2. Experimental data are from [42, 43].

between longitudinal and transverse cross sections. It should be noted, however, that this ratio could be changed if we decided to use different parameters for the resonance function in eq. (4.5) for the different polarizations.

Also in ϕ production our model agrees well with experimental data, as can be seen in figures 10 and 11. The qualitative properties are similar to those of ρ production

We note that the more stringent test of the hadronic component of the photon is obtained from DVCS. The ratio between vector meson production and DVCS is then more a test of the vector meson wavefunctions. It is therefore not surprising that we here get results similar to those in ref. [9]. The t-dependence presented in fig. 9 is, however, a result which in our model is sensitive to both the photon and vector meson wavefunctions, while

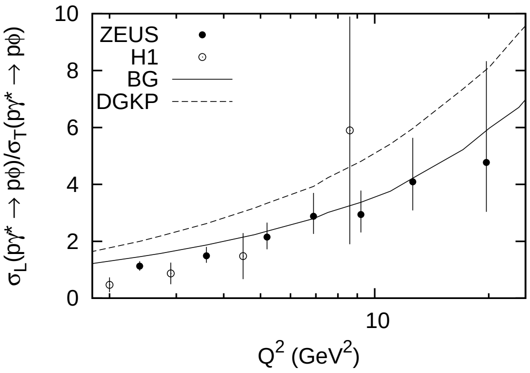

Figure 11: The ratio of longitudinal and transverse cross section for $\gamma^\star p \to \phi p$ as function of the photon virtuality at a center-of-mass energy of 75 GeV. Experimental data are from [42, 43].

in ref. [9] it was fixed by experimental data. From fig. 9 we see that for lower Q^2 the slope in the model is somewhat too steep, thus indicating a too wide wavefunction for the ρ meson. We see from figs. 1 and 2 that the ρ wavefunctions for transverse polarization are extending well beyond 5 GeV^{-1}. A faster falloff for large r-values would here give a better agreement with the observed t-dependence.

6.3 Exclusive ψ Production

In the case of ψ production we necessarily encounter more uncertainties. The result is sensitive to the mass of the charm quark, and here we use the value 1.4 GeV, which in the analysis in ref. [18] gave the correct charm contribution, F_2^c, to the proton structure function. We have not included a ψ component in the photon wave function, although this would in principle be possible. For the ψ meson wavefunction we use the parameters in table 1.

Our results are presented in figures 12 (dependence on Q^2 and W) and 13 (dependence on t). We note that the Boosted Gaussian wavefunction gives a too low cross section over the entire kinematic region, while DGKP model agrees very well both in its normalization and in its dependence on Q^2 and W. Both models show, however, a somewhat steeper t-dependence than the experimental data. This can be compared to the corresponding result for ρ meson production, and we conclude that also for the ψ meson the parameters in table 1 gives somewhat too wide wavefunctions.

7. Conclusions and Outlook

In this paper we have spent some effort on the modeling of non-perturbative aspects of the proton, photon and vector meson wavefunctions. None of our models are in any way unique or on solid theoretical grounds. However, they do allow us to compare our dipole evolution model directly to experimental data. Fixing the wavefunction parameters at one energy we find that the energy dependence of both total and (quasi-)elastic cross sections are well described by the cascade evolution, and rather independent of our modeling of the

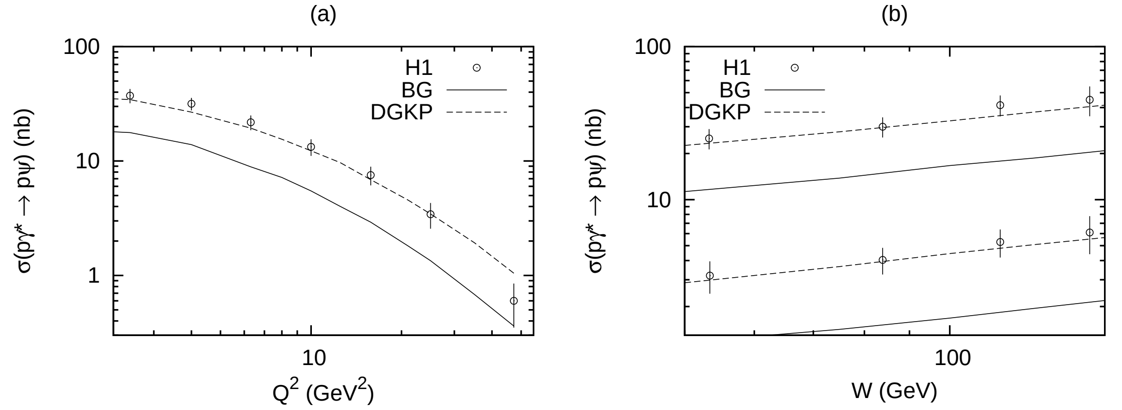

Figure 12: The cross section for $\gamma^\star p \to \psi p$ (a) As function of the photon virtuality at center-of-mass energy 90 GeV. The full and dashed line are with the two different meson wavefunction described in 4.3. (b) As function of center-of-mass energy for $Q^2 = 22.4$ GeV^2 (lower data) and 3.2 GeV^2 (upper data). Experimental data are from [44].

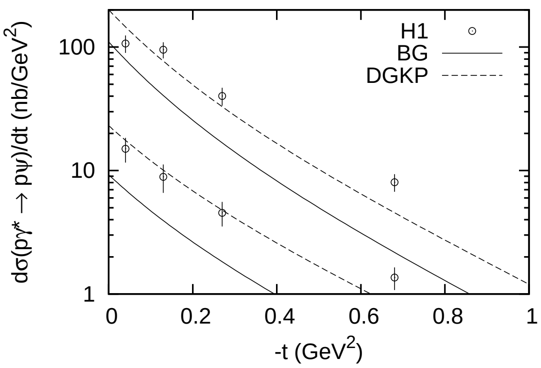

Figure 13: The cross section for $\gamma^\star p \to \psi p$ as function of transferred momentum squared t for $Q^2 = 22.4$ GeV^2 (lower data) and 3.2 GeV^2 (upper data). Experimental data are from [44].

wavefunctions. Also the slope in $d\sigma/dt$ for elastic pp scattering and DVCS is in agreement with experimental data independently of the tuning. This indicates a very high predictive power of our evolution model both when it comes to the average multiplicity and sizes of the dipoles (mainly influencing the total cross sections), the rate of increasing transverse size due to the dipole cascade (determining the energy variation of the dip position), and the fluctuations (mainly influencing the magnitude of elastic cross sections and their t-dependence).

Nevertheless, our modeling of the non-perturbative wavefunctions does give us valuable insights. Including the fluctuations in the cascade, the fluctuations in the proton wavefunction have to be rather small, in order to give the observed elastic cross section. The photon wavefunction clearly needs a hadronic component with a wavefunction with similar size as the proton and with similarly small fluctuations. The fact that the size comes out to be the same as the size of our proton may be a coincidence, but it could also indicate that there is a universal size of hadrons, at least when consisting of light quark flavours.

For the vector meson wavefunctions we have tested two different forms, which in the analysis by Forshaw *et al.* gave the best agreement with data for diffractive vector meson production. For light mesons the best result was obtained by the boosted Gaussian wavefunctions, while for ψ production the DGKP wavefunction was favored. In both cases the t-dependence was somewhat too steep, indicating that these wavefunctions extend out to too large r-values, where in particular the wavefunctions for transverse polarization are much wider than our wavefunctions for the proton and the photon.

The robustness of our model for dipole evolution, both for inclusive and exclusive cross sections increases our confidence that it can be used to also model fully exclusive final states. In future publications we will therefore concentrate on turning our Monte Carlo simulation program into a full-fledged event generator, which would then be able to model multi-particle production at e.g. the LHC, with special emphasis on the underlying event and multiple scatterings.

Acknowledgment

We want to thank Emil Avsar for valuable discussions. This work is supported in part by the Marie Curie research training network "MCnet" (contract number MRTN-CT-2006-035606) and by the Swedish Foundation for International Cooperation and Higher Education – STINT, contract number 2006/080. Gösta Gustafson also acknowledges support from the Deutsche Forschungsgemeinschaft.

References

[1] E. Avsar, G. Gustafson, and L. Lönnblad *JHEP* **07** (2005) 062, `hep-ph/0503181`.

[2] E. Avsar, G. Gustafson, and L. Lonnblad *JHEP* **01** (2007) 012, `hep-ph/0610157`.

[3] E. Avsar, G. Gustafson, and L. Lonnblad *JHEP* **12** (2007) 012, `arXiv:0709.1368 [hep-ph]`.

[4] A. H. Mueller *Nucl. Phys.* **B415** (1994) 373–385.

[5] A. H. Mueller and B. Patel *Nucl. Phys.* **B425** (1994) 471–488, `hep-ph/9403256`.

[6] A. H. Mueller *Nucl. Phys.* **B437** (1995) 107–126, `hep-ph/9408245`.

[7] G. P. Salam *Comput. Phys. Commun.* **105** (1997) 62–76, `hep-ph/9601220`.

[8] A. H. Mueller and G. P. Salam *Nucl. Phys.* **B475** (1996) 293–320, `hep-ph/9605302`.

[9] J. R. Forshaw, R. Sandapen, and G. Shaw *Phys. Rev.* **D69** (2004) 094013, `hep-ph/0312172`.

[10] J. R. Forshaw, R. Sandapen, and G. Shaw *JHEP* **11** (2006) 025, `hep-ph/0608161`.

[11] J. Kwiecinski, A. D. Martin, and P. J. Sutton *Z. Phys.* **C71** (1996) 585–594, `hep-ph/9602320`.

[12] I. Balitsky *Phys. Rev.* **D75** (2007) 014001, `hep-ph/0609105`.

[13] Y. V. Kovchegov and H. Weigert *Nucl. Phys.* **A789** (2007) 260–284, `hep-ph/0612071`.

[14] I. Balitsky. Talk presented at the ISMD07, Berkeley, August 2007, see http://www-rnc.lbl.gov/ISMD/.

[15] M. Praszalowicz and A. Rostworowski *Acta Phys. Polon.* **B29** (1998) 745–753, hep-ph/9712313.

[16] M. Glück, E. Reya, and A. Vogt *Eur. Phys. J.* **C5** (1998) 461–470, hep-ph/9806404.

[17] H. Kowalski and D. Teaney *Phys. Rev.* **D68** (2003) 114005, hep-ph/0304189.

[18] E. Avsar and G. Gustafson *JHEP* **04** (2007) 067, hep-ph/0702087.

[19] L. Frankfurt, V. Guzey, and M. Strikman *Phys. Rev.* **D58** (1998) 094039, hep-ph/9712339.

[20] H. G. Dosch, T. Gousset, G. Kulzinger, and H. J. Pirner *Phys. Rev.* **D55** (1997) 2602–2615, hep-ph/9608203.

[21] M. Wirbel, B. Stech, and M. Bauer *Z. Phys.* **C29** (1985) 637.

[22] S. J. Brodsky, T. Huang, and G. P. Lepage. Shorter version contributed to 20th Int. Conf. on High Energy Physics, Madison, Wisc., Jul 17-23, 1980.

[23] J. Nemchik, N. N. Nikolaev, E. Predazzi, and B. G. Zakharov *Z. Phys.* **C75** (1997) 71–87, hep-ph/9605231.

[24] **CDF** Collaboration, F. Abe *et al. Phys. Rev.* **D50** (1994) 5518–5534.

[25] **CDF** Collaboration, F. Abe *et al. Phys. Rev.* **D50** (1994) 5550–5561.

[26] **E-710** Collaboration, N. A. Amos *et al. Phys. Lett.* **B243** (1990) 158–164.

[27] **E-811** Collaboration, C. Avila *et al. Phys. Lett.* **B537** (2002) 41–44.

[28] **UA4/2** Collaboration, C. Augier *et al. Phys. Lett.* **B344** (1995) 451–454.

[29] M. M. Block, F. Halzen, and T. Stanev *Phys. Rev.* **D62** (2000) 077501, hep-ph/0004232.

[30] A. Donnachie and P. V. Landshoff *Phys. Lett.* **B296** (1992) 227–232, hep-ph/9209205.

[31] M. G. Ryskin, A. D. Martin, and V. A. Khoze *Eur. Phys. J.* **C54** (2008) 199–217, 0710.2494.

[32] **E-710** Collaboration, N. A. Amos *et al. Phys. Lett.* **B247** (1990) 127–130.

[33] **UA4** Collaboration, D. Bernard *et al. Phys. Lett.* **B171** (1986) 142.

[34] **NA22** Collaboration, M. Adamus *et al. Phys. Lett.* **B186** (1987) 223–226.

[35] J. R. Forshaw, G. Kerley, and G. Shaw *Phys. Rev.* **D60** (1999) 074012, hep-ph/9903341.

[36] **ZEUS** Collaboration, S. Chekanov *et al. Nucl. Phys.* **B713** (2005) 3–80, hep-ex/0501060.

[37] **H1** Collaboration, A. Aktas *et al. Eur. Phys. J.* **C44** (2005) 1–11, hep-ex/0505061.

[38] **H1** Collaboration, F. D. Aaron *et al. Phys. Lett.* **B659** (2008) 796–806, 0709.4114.

[39] **H1** Collaboration, C. Adloff *et al. Eur. Phys. J.* **C13** (2000) 371–396, hep-ex/9902019.

[40] **ZEUS** Collaboration, S. Chekanov *et al. PMC Phys.* **A1** (2007) 6, 0708.1478.

[41] **ZEUS** Collaboration, J. Breitweg *et al. Eur. Phys. J.* **C6** (1999) 603–627, hep-ex/9808020.

[42] **H1** Collaboration, C. Adloff *et al. Phys. Lett.* **B483** (2000) 360–372, hep-ex/0005010.

[43] **ZEUS** Collaboration, S. Chekanov *et al. Nucl. Phys.* **B718** (2005) 3–31, hep-ex/0504010.

[44] **H1** Collaboration, A. Aktas *et al. Eur. Phys. J.* **C46** (2006) 585–603, hep-ex/0510016.